

# Out-of-equilibrium phase transitions in the HMF model: a closer look

F. Staniscia,<sup>1,2</sup> P.H. Chavanis,<sup>3</sup> and G. De Ninno<sup>2,4</sup>

<sup>1</sup>*Dipartimento di Fisica, Università di Trieste, 34127 Trieste, Italy*

<sup>2</sup>*Sincrotrone Trieste, S.S. 14 km 163.5, Basovizza, 34149 Trieste, Italy*

<sup>3</sup>*Laboratoire de Physique Théorique (IRSAMC), Université de Toulouse (UPS) and CNRS, F-31062 Toulouse, France*

<sup>4</sup>*Physics Department, Nova Gorica University 5001 Nova Gorica, Slovenia*

We provide a detailed discussion of out-of-equilibrium phase transitions in the Hamiltonian Mean Field (HMF) model in the framework of Lynden-Bell's statistical theory of the Vlasov equation. For two-levels initial conditions, the caloric curve  $\beta(E)$  only depends on the initial value  $f_0$  of the distribution function. We evidence different regions in the parameter space where the nature of phase transitions between magnetized and non-magnetized states changes: (i) for  $f_0 > 0.10965$ , the system displays a second order phase transition; (ii) for  $0.109497 < f_0 < 0.10965$ , the system displays a second order phase transition and a first order phase transition; (iii) for  $0.10947 < f_0 < 0.109497$ , the system displays two second order phase transitions; (iv) for  $f_0 < 0.10947$ , there is no phase transition. The passage from a first order to a second order phase transition corresponds to a tricritical point. The sudden appearance of two second order phase transitions from nothing corresponds to a second order azeotropy. This is associated with a phenomenon of phase reentrance. When metastable states are taken into account, the problem becomes even richer. In particular, we find a new situation of phase reentrance. We consider both microcanonical and canonical ensembles and report the existence of a tiny region of ensembles inequivalence. We also explain why the use of the initial magnetization  $M_0$  as an external parameter, instead of the phase level  $f_0$ , may lead to inconsistencies in the thermodynamical analysis.

PACS numbers:

## I. INTRODUCTION

Systems with long-range interactions have recently been the object of an intense activity [1–4]. These systems are numerous in nature and concern different disciplines such as astrophysics (galaxies) [5–7], two-dimensional turbulence (vortices) [8–10], biology (chemotaxis) [11], plasma physics [12–14] and modern technologies such as Free Electron Lasers (FEL) [15–17]. In addition, their study is interesting at a conceptual level because it obliges to go back to the foundations of statistical mechanics and kinetic theory [4, 18–20]. Indeed, systems with long-range interactions exhibit a number of unusual features that are not present in systems with short-range interactions. For example, their equilibrium statistical mechanics is marked by the existence of spatially inhomogeneous equilibrium states [1], unusual thermodynamic limits [21–23], inequivalence of statistical ensembles [5, 7, 24], negative specific heats [25, 26], various kinds of phase transitions [7, 27] etc. Their dynamics is also very interesting because these systems can be found in long-lived quasi stationary states (QSS) that are different from Boltzmann equilibrium states. These QSSs can be interpreted as stable steady states of the Vlasov equation which governs the evolution of the system for sufficiently “short” times before correlations have developed [12, 28]. In fact, for systems with long-range interactions, the collisional relaxation time towards the Boltzmann distribution increases rapidly with the number of particles  $N$  and diverges at the thermodynamic limit  $N \rightarrow +\infty$  [4, 19, 20, 28]. Therefore, the domain of validity of the Vlasov equation is huge and the QSSs

have very long lifetimes. In many cases, they are the only observable structures in a long-range system, so that they are often more physically relevant than the Boltzmann equilibrium state itself. A question that naturally emerges is whether one can predict the QSS actually reached by the system. This is not an easy task since the Vlasov equation admits an infinite number of stable steady states in which the system can be trapped [28]. In a seminal paper, Lynden-Bell [29] proposed to determine the QSS eventually reached by the system by developing a statistical mechanics of the Vlasov equation. To that purpose, he introduced the notions of phase mixing, violent relaxation and coarse-grained distributions. He obtained the most probable distribution by maximizing a Boltzmann-type entropy while conserving all the constraints of the Vlasov equation (in particular the infinite class of Casimirs). By definition, this “most mixed state” is the statistical equilibrium state of the Vlasov equation (at a coarse-grained scale). Whether or not the system truly reaches this equilibrium state relies on an assumption of ergodicity and efficient mixing. This ergodicity assumption is not always fulfilled in the process of violent relaxation and the Lynden-Bell prediction may fail. In that case, the QSS can be another stable steady state of the Vlasov equation that is incompletely mixed. This is referred to as incomplete relaxation (see, e.g. [30], for discussion and further references). In case of incomplete relaxation, the prediction of the QSS is very difficult, and presumably impossible. Nevertheless, in many cases, the Lynden-Bell approach gives a fine first order prediction of the achieved QSS and allows one to predict out-of-equilibrium phase transitions between different types of structures that can be compared with direct simula-

tions or experiments. Before addressing this problem in a specific situation, namely the Hamiltonian Mean Field (HMF) model [31, 32], let us first briefly review the successes and the weaknesses of the Lynden-Bell approach.

Lynden-Bell’s statistical theory of violent relaxation was elaborated in the context of 3D stellar systems. Unfortunately, this is the worse situation for its practical application. Indeed, the predicted distribution function has infinite mass (the spatial density decreases at large distances like  $r^{-2}$ ). In other words, this means that there is no entropy maximum for a stellar system in an infinite domain [28]. This is a clear evidence of the fact that galaxies have necessarily reached a state of *incomplete* violent relaxation. In fact, the Lynden-Bell theory is able to explain the isothermal core of elliptical galaxies without recourse to collisions that operate on a much longer timescale (of the order of the Chandrasekhar relaxation time [33]). This is usually recognized as a major success of the theory. Unfortunately, it fails at predicting the structure of the halo whose velocity distribution is anisotropic and whose spatial density decreases like  $r^{-4}$  [28]. Models of incomplete violent relaxation have been elaborated by Bertin & Stiavelli [34], Stiavelli & Bertin [35] and Hjorth & Madsen [36]. These models are able to reproduce the de Vaucouleurs law of elliptical galaxies and provide a very good agreement with numerical simulations up to nine orders of magnitude [37]. Another possibility to describe incomplete relaxation is to develop a kinetic theory of violent relaxation in order to understand what limits mixing [38–40]. The idea is that, in case of incomplete relaxation (non-ergodicity), the prediction of the QSS is impossible without considering the dynamics [30]. Finally, in more academic studies [41], one can confine the system within an artificial spherical box and assume a complete relaxation inside the box. Since the Lynden-Bell distribution is similar to the Fermi-Dirac statistics (in the two-levels approximation), the problem is mathematically equivalent to the study of a gas of self-gravitating fermions in a box. This theoretical problem has been studied in detail by Chavanis [42]. The caloric curve  $\beta(E)$  displays a rich variety of microcanonical and canonical phase transitions (zeroth and first order) between gaseous (non degenerate) and condensed (degenerate) states, depending on the value of a degeneracy parameter related to the initial distribution function  $f_0$  in the Lynden-Bell theory. In particular, there exists two critical points in the phase diagram, one in each ensemble, at which the phase transitions are suppressed. For details about these phase transitions, and for an extended bibliography, we refer to the review [7]. The Lynden-Bell prediction has also been tested in 1D and 2D gravity [43, 44] where the infinite mass problem does not arise [45]. However, it is found again that relaxation is incomplete and that the Lynden-Bell prediction fails [89]. Finally, Arad & Lynden-Bell [46] have shown that the theory itself presents some inconsistencies arising from its non-transitive nature. These negative results have led many astrophysicists to the conclusion that the

Lynden-Bell theory does not work in practice [28].

A similar statistical theory has been developed by Miller [47], and independently by Robert & Sommeria [48], in 2D turbulence in order to explain the robustness of long-lived vortices in astrophysical and geophysical flows (a notorious example being Jupiter’s great red spot). Large-scale vortices are interpreted as quasi stationary states of the 2D Euler equation in the same way that galaxies are quasi stationary states of the Vlasov equation (see [10, 49] for a discussion of the numerous analogies between the statistical mechanics and the kinetic theory of 2D vortices and stellar systems). Miller-Robert-Sommeria (MRS) developed a statistical theory of the 2D Euler equation in order to predict the most probable state achieved by the system. Although situations of incomplete relaxation have also been evidenced in 2D turbulence [50–52], the MRS theory has met a lot of success. For example, it is able to account for geometry induced phase transitions between monopoles and dipoles as we change the aspect ratio of the domain [53–57]. Phase transitions and bifurcations between different types of flows have also been studied in [58–60]. On the other hand, when applied to geophysical and astrophysical flows, the MRS theory is able to account for the structure and the organization of large-scale flows such as jovian jets and vortices [61–64] and Fofonoff flows in oceanic basins [55, 65]. This theory has also been applied to more complicated situations such as 2D magnetohydrodynamics (MHD) [66, 67] and axisymmetric flows (the celebrated von Kármán flow) [68].

A toy model of systems with long-range interactions, called the Hamiltonian Mean Field (HMF) model, has been introduced in statistical physics [31, 32] and extensively studied [4]. It can be viewed as a  $XY$  spin system with infinite range interactions or as a one dimensional model of particles moving on a ring and interacting via a long-range potential truncated to one Fourier mode (cosine potential). In that second interpretation, it shares many analogies with self-gravitating systems [31, 32, 69] but is much simpler to study since it avoids difficulties linked with the singular nature of the gravitational potential at the origin and the absence of a natural confinement [5–7]. The observation of quasi stationary states in the HMF model [32, 70] was a surprise in the community of statistical mechanics working on systems with long-range interactions. It was recognized early that these QSSs are out-of-equilibrium structures and that they are non-Boltzmannian. They were first interpreted [70] in terms of Tsallis generalized thermodynamics [71] with the argument that the system is nonextensive so that Boltzmann statistical mechanics is not applicable. Later, inspired by analogies with stellar systems and 2D vortices reported in [10], different groups started to interpret these QSSs in terms of stable steady states of the Vlasov equation and statistical equilibrium states in the sense of Lynden-Bell [69, 72, 73]. Chavanis [74] studied out-of-equilibrium phase transitions in the HMF model by analogy with similar studies in astrophysics and hydro-

dynamics [41, 53] and obtained a phase diagram in the  $(f_0, E)$  plane [90] between magnetized ( $M \neq 0$ ) and non-magnetized ( $M = 0$ ) states. These regions are separated by a critical line  $E_c(f_0)$  that marks the domain of stability of the homogeneous phase. This critical line displays a turning point at  $((f_0)_*, E_*) \simeq (0.10947, 0.608)$  leading to a phenomenon of *phase reentrance* (as we reduce the energy, the homogeneous phase is successively stable, unstable and stable again). Antoniazzi *et al.* [75] studied the validity of the Lynden-Bell prediction by performing careful comparisons with direct  $N$ -body simulations at  $E = 0.69$  and found a good agreement for initial magnetizations  $M_0 < (M_0)_{crit}(E) \simeq 0.897$  leading to spatially homogeneous Lynden-Bell distributions [91]. Antoniazzi *et al.* [78] obtained a phase diagram in the  $(M_0, E)$  plane and showed that the system exhibits first and second order phase transitions separated by a tricritical point. Finally, Antoniazzi *et al.* [79] performed numerical simulations of the Vlasov equation and found a good agreement with direct  $N$ -body simulations and Lynden-Bell's prediction for the explored range of parameters. A synthesis of these results was published in [80]. In this paper, a more detailed discussion of phase transitions in the  $(f_0, E)$  plane was given, showing the lines of first and second order phase transitions and the domains of metastability. On the other hand, a comparison between the phase diagrams in the  $(f_0, E)$  and  $(M_0, E)$  planes was made. It was stated, without rigorous justification, that the tricritical point in the  $(M_0, E)$  plane corresponds to the turning point of the critical line  $E_c(f_0)$  in the  $(f_0, E)$  plane, i.e. the point where the phase reentrance starts. These results were confronted to numerical simulations by Staniscia *et al.* [81]. These simulations confirmed the existence of a reentrant phase in the very narrow region predicted by the theory [74] but also showed discrepancies with the Lynden-Bell prediction (such as an additional reentrant phase and a persistence of magnetized states in the *a priori* non-magnetized region) that were interpreted as a result of incomplete relaxation. Staniscia *et al.* [81] also determined the physical caloric curve  $\beta_{kin}(E)$ , where  $\beta_{kin} = 1/T_{kin}$  is the inverse kinetic temperature, in the region of the phase diagram displaying first and second order phase transitions, and reported the existence of a region of negative kinetic specific heat  $C_{kin} = dE/dT_{kin} < 0$ . In a recent paper [82], the thermodynamical caloric curve  $\beta(E)$  was determined in the same region of parameters and it was shown that the thermodynamical specific heat  $C = dE/dT$  is always positive, even in the region where the kinetic specific heat is negative. In particular, it is argued that the ensembles are equivalent although the experimentally measured specific heat is negative [92].

These various results show that the description of out-of-equilibrium phase transitions in the HMF model is extremely rich and subtle. In this paper, we describe in more detail the phase transitions between magnetized and non-magnetized states in the  $(f_0, E)$  plane. In particular, we plot the series of equilibria  $\beta(E)$  for differ-

ent values of  $f_0$  and determine the caloric curve corresponding to fully stable states. This completes and illustrates our previous study [81] where only the final phase diagram was reported. We evidence different regions in the parameter space where the nature of phase transitions changes: (i) for  $f_0 > (f_0)_t \simeq 0.10965$ , the system displays a second order phase transition; (ii) for  $(f_0)_1 \simeq 0.109497 < f_0 < (f_0)_t \simeq 0.10965$ , the system displays a second order phase transition and a first order phase transition; (iii) for  $(f_0)_* \simeq 0.10947 < f_0 < (f_0)_1 \simeq 0.109497$ , the system displays two second order phase transitions; (iv) for  $f_0 < (f_0)_* \simeq 0.10947$ , there is no phase transition. The passage from a first order phase transition to a second order phase transition corresponds to a tricritical point. The sudden appearance of two second order phase transitions from nothing corresponds to a second order azeotropy. This is associated with a phenomenon of phase reentrance. When we take into account metastable states, the description is even richer and seven regions must be considered (see Sec. III). In particular, we find a new situation of phase reentrance. We also stress two unexpected results that were not reported (or incorrectly reported) in previous works: (i) Contrary to what is stated in [82], there exists a region of ensembles inequivalence but it concerns an extremely narrow range of parameters so that the conclusions of [82] are not altered; (ii) the tricritical point separating second and first order phase transitions does not exactly coincide with the turning point of the stability line  $E_c(f_0)$ , contrary to what is stated in [80], but is slightly different. Again, the difference is small so that the main results of previous works are not affected. However, this slight difference leads to an even richer variety of phase transitions. We may be fascinated by the fact that so many things happen in such a very narrow range of parameters (typically  $(f_0)_m \simeq 0.1075 < f_0 < (f_0)_c \simeq 0.11253954$ ) although  $f_0$  can take *a priori* any value between 0 and  $+\infty$ ! Finally, we make clear in this paper (see Sec. II) that the relevant control parameters associated with the Lynden-Bell theory are  $(f_0, E)$  [74] while the use of the variables  $(M_0, E)$  [78, 79] may lead to physical inconsistencies in the thermodynamical analysis.

## II. THE LYNDEN-BELL THEORY AND THE CHOICE OF THE CONTROL PARAMETERS

The HMF model [31, 32], which shares many similarities with gravitational and charged sheet models, describes the one-dimensional motion of  $N$  particles of unit mass moving on a unit circle and coupled through a mean field cosine interaction. The system Hamiltonian reads

$$H = \frac{1}{2} \sum_{i=1}^N v_i^2 + \frac{1}{2N} \sum_{i,j=1}^N [1 - \cos(\theta_i - \theta_j)], \quad (1)$$

where  $\theta_i$  represents the angle that particle  $i$  makes with an axis of reference and  $v_i$  stands for its velocity. The

$1/N$  factor in front of the potential energy corresponds to the Kac prescription to make the system extensive and justify the validity of the mean field approximation in the limit  $N \rightarrow +\infty$ . The relevant order parameter is the magnetization defined as  $\mathbf{M} = (\sum_i \mathbf{m}_i)/N$  where  $\mathbf{m}_i = (\cos \theta_i, \sin \theta_i)$ . In the  $N \rightarrow +\infty$  limit, the time evolution of the one body distribution function  $f(\theta, v, t)$  is governed by the Vlasov equation

$$\frac{\partial f}{\partial t} + v \frac{\partial f}{\partial \theta} - (M_x[f] \sin \theta - M_y[f] \cos \theta) \frac{\partial f}{\partial v} = 0, \quad (2)$$

where  $M_x[f] = \int f(\theta, v, t) \cos \theta d\theta dv$  and  $M_y[f] = \int f(\theta, v, t) \sin \theta d\theta dv$  are the two components of the magnetization.

The statistical theory of the Vlasov equation, introduced by Lynden-Bell [29], has been reviewed in several papers [4, 18, 74, 75, 80, 81] so that we shall here only recall the main lines that are important to understand the sequel. We assume that the initial distribution function takes only two values  $f(\theta, v, t=0) \in \{0, f_0\}$ . For example, it can be made of one or several patches of uniform distribution  $f(\theta, v, 0) = f_0$  surrounded by ‘‘vacuum’’  $f(\theta, v, 0) = 0$ . We note that the number and the shape of these patches can be completely arbitrary. For such initial conditions, the quantities conserved by the Vlasov equation are: (i) the value  $f_0$  of the initial distribution; (ii) the normalization  $\mathcal{M} = \int f d\theta dv = 1$ ; (iii) the energy  $E = \frac{1}{2} \int f v^2 d\theta dv + \frac{1}{2}(1 - M^2)$ . The fine-grained distribution function  $f(\theta, v, t)$  is stirred in phase space but conserves its two values  $f_0$  and 0 at any time, i.e.  $f(\theta, v, t) \in \{0, f_0\} \forall t$ . However, as time goes on, the two levels values  $f_0$  and 0 become more and more intermingled as a result of a mixing process (filamentation) in phase space. The coarse-grained distribution  $\bar{f}(\theta, v, t)$ , which can be viewed as a local average of the fine-grained distribution function, takes values intermediate between 0 and  $f_0$ , i.e.  $0 \leq \bar{f}(\theta, v, t) \leq f_0$ . It is expected to achieve a steady state  $\bar{f}(\theta, v)$  as a result of violent relaxation on a relatively short timescale (a few dynamical times). This corresponds to the QSS observed in the simulations. The most probable, or most mixed state, is obtained by maximizing the Lynden-Bell entropy

$$S = - \int \left[ \frac{\bar{f}}{f_0} \ln \frac{\bar{f}}{f_0} + \left(1 - \frac{\bar{f}}{f_0}\right) \ln \left(1 - \frac{\bar{f}}{f_0}\right) \right] d\theta dv, \quad (3)$$

while conserving  $E$  and  $\mathcal{M}$  (for a given value of  $f_0$ ). This determines the statistical equilibrium state of the Vlasov equation. Note that the whole theory relies on an assumption of ergodicity, i.e. efficient mixing. Our aim here is not to determine the range of validity of the Lynden-Bell theory, so that we shall assume that this assumption is fulfilled (see, e.g. [77], for a discussion of incomplete relaxation in the HMF model). We are led therefore to considering the maximization problem

$$\max_{\bar{f}} \{S[\bar{f}] \mid E[\bar{f}] = E, \mathcal{M}[\bar{f}] = 1\}, \quad (4)$$

for a given value of  $f_0$ . The critical points of (4), canceling the first order variations of the constrained entropy, are given by the variational principle

$$\delta S - \beta \delta E - \alpha \delta \mathcal{M} = 0, \quad (5)$$

where  $\beta$  and  $\alpha$  are Lagrange multipliers. This yields the Lynden-Bell distribution

$$\bar{f}_{LB}(\theta, v) = \frac{f_0}{1 + e^{\beta f_0 \epsilon(\theta, v) + f_0 \alpha}}, \quad (6)$$

where  $\epsilon(\theta, v) = v^2/2 - M_x[\bar{f}_{LB}] \cos \theta - M_y[\bar{f}_{LB}] \sin \theta$  is the individual energy. In the two-levels approximation, the Lynden-Bell distribution is formally identical to the Fermi-Dirac statistics [29]. Note that  $T = \beta^{-1} = (\partial S / \partial E)^{-1}$  is the *thermodynamical temperature*. Since the distribution function (6) is non-Boltzmannian, the thermodynamical temperature differs from the *classical kinetic temperature*  $T_{kin} = \int f v^2 d\theta dv$ . This point has been studied specifically in [82].

The maximization problem (4) corresponds to the microcanonical ensemble (MCE). Since the Lynden-Bell theory is based on the Vlasov equation that describes an isolated system, the microcanonical ensemble is the relevant ensemble to consider (the energy is fixed). We can, however, formally define a canonical ensemble. We introduce the free energy functional  $J[\bar{f}] = S[\bar{f}] - \beta E[\bar{f}]$  [93] and consider the maximization problem

$$\max_{\bar{f}} \{J[\bar{f}] \mid \mathcal{M}[\bar{f}] = 1\}, \quad (7)$$

for a given value of  $f_0$ . The maximization problems (4) and (7) have the same critical points since the variational principle

$$\delta J - \alpha \delta \mathcal{M} = 0 \quad (8)$$

returns Eq. (5) (recall that  $\beta$  is fixed in the canonical ensemble). In addition, it can be shown at a general level [24] that a solution of the canonical problem (7) is always a solution of the more constrained dual microcanonical problem (4), but that the reciprocal is wrong in case of ensembles inequivalence [94]. Therefore, even if the canonical ensemble is not physically justified in the context of Lynden-Bell’s theory of violent relaxation, it provides nevertheless a *sufficient* condition of microcanonical thermodynamical stability. It is therefore useful in that respect. In addition, it is interesting on a conceptual point of view to study possible inequivalence between microcanonical and canonical ensembles. Therefore, we shall study in this paper the two maximization problems (4) and (7), while emphasis and illustrations will be given for the more physical microcanonical case.

Before that, let us recall general notions that will be useful in the sequel (for an extended account, see e.g. [7]). For a given value of  $f_0$ , the *series of equilibria* is the curve  $\beta(E)$  containing all the *critical points* of (4)

or (7) (as we have seen, they are the same). The stable part of this curve, in each ensemble, gives the corresponding *caloric curve*. In MCE, the control parameter is the energy and the stable states are maxima of entropy  $S$  at fixed energy and normalization. This defines the microcanonical caloric curve  $\beta(E)$ . In CE, the control parameter is the inverse temperature and the stable states are maxima of free energy  $J$  at fixed normalization. This defines the canonical caloric curve  $E(\beta)$ . The *strict caloric curve* contains only *fully stable states* ( $S$ ) that are global entropy maxima at fixed energy and normalization in MCE or global free energy maxima at fixed normalization in CE. The *physical caloric curve* contains fully stable and *metastable states* ( $M$ ), that are local entropy maxima at fixed energy and normalization in MCE or local free energy maxima at fixed normalization in CE. The *unstable states* ( $U$ ), that are minima or saddle points of the thermodynamical potential, must be rejected. Note that for systems with long-range interactions, metastable states can have very long lifetimes so that they are very important in practice. By studying the caloric curve  $\beta(E)$  for a given value of  $f_0$ , we can describe *phase transitions*. Microcanonical first order phase transition are marked by the discontinuity of the inverse temperature  $\beta(E)$  at some energy  $E_t$ . This corresponds to a discontinuity of the first derivative of entropy  $S'(E) = \beta(E)$  at  $E_t$  in the energy vs entropy curve. There can exist metastable branches around  $E_t$  that possibly end at microcanonical *spinodal points*. Microcanonical second order phase transitions are marked by the discontinuity of  $\beta'(E)$  at some energy  $E_c$ . This corresponds to a discontinuity of the second derivative of entropy  $S''(E) = \beta'(E)$  at  $E_c$ . Similarly, canonical first order phase transitions are marked by the discontinuity of energy  $E(\beta)$  at some inverse temperature  $\beta_t$ . This corresponds to a discontinuity of the first derivative of free energy  $J'(E) = -E(\beta)$  at  $\beta_t$  in the inverse temperature vs free energy curve. There can exist metastable branches around  $\beta_t$  that possibly end at canonical spinodal points. Canonical second order phase transitions are marked by the discontinuity of  $E'(\beta)$  at some inverse temperature  $\beta_c$ . This corresponds to a discontinuity of the second derivatives of free energy  $J''(\beta) = -E'(\beta)$  at  $\beta_c$ . Finally, by varying the *external parameter*  $f_0$ , we can describe changes from different kinds of phase transitions at some *critical values* of  $f_0$  and plot the corresponding *phase diagrams*  $(f_0, E)$  and  $(f_0, \beta)$  in microcanonical and canonical ensembles. This is the program that we shall follow in this paper.

We emphasize that these general results are valid for the caloric curve  $\beta(E)$  where  $\beta$  is the inverse thermodynamical temperature, not the inverse kinetic temperature. In particular, the thermodynamical specific heat  $C = dE/dT$  is always positive in the canonical ensemble while the kinetic specific heat  $C_{kin} = dE/dT_{kin}$  can be positive or negative in the canonical ensemble. This has been illustrated in [82].

A last comment is in order. If we consider a waterbag

initial condition in which  $f(\theta, v, t = 0) = f_0$  in the rectangle  $[\theta_{min}, \theta_{max}] \times [-v_{min}, v_{max}]$  and  $f(\theta, v, t = 0) = 0$  outside, it seems convenient to take as control parameters the initial magnetization  $M_0$  and the energy  $E$  as done in [78, 79]. Indeed, the specification of these parameters determines  $f_0 = \phi(E, M_0)$  and  $E$  and thus allows to compute the corresponding Lynden-Bell state. Therefore, it seems that the choice of the control parameters  $(E, M_0)$  or  $(E, f_0)$  is just a question of commodity. In fact, this is not the case, and we would like to point out some difficulties in taking  $(E, M_0)$  as control parameters in the thermodynamical analysis:

(i) The control parameters  $(E, M_0)$  are less general than  $(E, f_0)$  because they assume that the initial condition is a waterbag distribution, whereas the control parameters  $(E, f_0)$  are valid for *any* initial distribution with two levels, whatever the number of patches and their shape. They allow therefore to describe a wider class of situations.

(ii) The variables  $(E, M_0)$  may lead to redundancies because there may exist two (or more) couples  $(E, M_0^{(1)})$  and  $(E, M_0^{(2)})$  that correspond to the *same*  $(E, f_0)$  and, consequently, to the *same* Lynden-Bell state (recall that the Lynden-Bell prediction only depends on  $E$  and  $f_0$ ) [95]. This has been illustrated in [80, 81].

(iii) More importantly, the use of  $M_0$  as an external parameter (instead of  $f_0$ ) leads to physical inconsistencies in the thermodynamical analysis. Indeed, if we work in terms of the variables  $(E, M_0)$ , the initial value of the distribution  $f_0$  becomes a function  $f_0 = \phi(E, M_0)$  of these variables. As a result, the Lynden-Bell entropy functional

$$S = - \int \left[ \frac{\bar{f}}{\phi(E, M_0)} \ln \frac{\bar{f}}{\phi(E, M_0)} + \left( 1 - \frac{\bar{f}}{\phi(E, M_0)} \right) \ln \left( 1 - \frac{\bar{f}}{\phi(E, M_0)} \right) \right] d\theta dv, \quad (9)$$

depends not only of the external parameter  $M_0$  but also on the energy  $E$ . This is clearly a very unconventional situation. Indeed, if we want to apply the standard results recalled above, the entropic functional can depend on an external parameter but it cannot explicitly depend on the energy. Therefore, these general results [24] are not valid for functionals of the form (9). In particular, the “improper” caloric curve  $\beta(E)$  at fixed  $M_0$  can display a region of negative specific heat while the proper caloric curve  $\beta(E)$  at fixed  $f_0$  does not. This is exemplified in Fig. 1(b) of [79] where the entropy versus energy is plotted at fixed  $M_0$ . This curve has a convex dip (revealing a negative specific heat region), while the curve  $S(E)$  at fixed  $f_0$  has no convex dip and the ensembles are equivalent [82].

Finally, in the other contexts where the Lynden-Bell theory has been applied [41, 52, 58–60, 63], the control parameters that have been taken are  $E$  and  $f_0$ . It is therefore important to describe the phase transitions in terms of these parameters as initiated in [74].

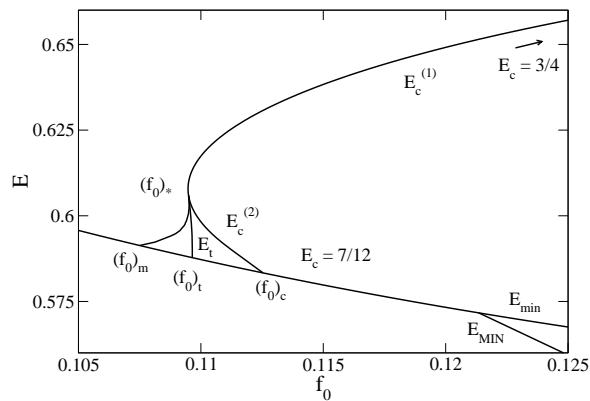


FIG. 1: Phase diagram in the microcanonical ensemble. We have indicated several representative points. The minimum accessible energy of the homogeneous phase, corresponding to a waterbag (or Fermi) distribution, is  $E_{min}(f_0) = 1/(96\pi^2 f_0^2) + 1/2$  [74, 80]. We have also indicated the minimum accessible energy (for homogeneous and inhomogeneous phases) in the case where the initial condition is a rectangular waterbag initial condition. It is equal to  $E_{min}(f_0)$  when  $f_0 < 0.12135\dots$  and to  $E_{MIN}(f_0)$  when  $f_0 > 0.12135\dots$  (see [81] for details). The curves  $E_t(f_0)$  and  $E_m(f_0)$  have been continued “by hand” (due to numerical problems) and may not be correct for small energies (see Appendix A).

### III. DESCRIPTION OF CALORIC CURVES AND PHASE TRANSITIONS

#### A. Phase diagrams

In Fig. 1, we reproduce the microcanonical phase diagram obtained in [81]. In Fig. 2, we enlarge this diagram close to the turning point of energy  $((f_0)_*, E_*) \simeq (0.10947, 0.608)$  in order to show that its structure is more complicated than previously thought. Similarly, in Figs. 3 and 4, we plot the canonical phase diagram and its enlargement close to the turning point of temperature  $((f_0)_*, \beta_*) \simeq (0.10947, 118)$ . These phase diagrams show that we must consider different regions where the nature of phase transitions changes.

In the following sections, we plot the series of equilibria  $\beta(E)$  in seven characteristic regions of the phase diagram and describe the corresponding phase transitions. The branches (S) correspond to fully stable states, the branches (M) correspond to metastable states and the branches (U) correspond to unstable states. At the end of each subsection, we summarize the nature of phase transitions in the corresponding region by considering only fully stable states.

We will find that the microcanonical and canonical phase transitions are very similar. In fact, the ensembles differ only in a very small range of parameters. Therefore, we will essentially focus on the microcanonical ensemble and only mention the canonical ensemble in case of ensembles inequivalence.

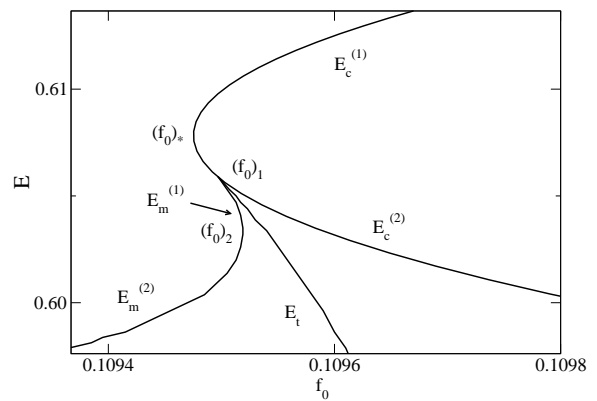


FIG. 2: Enlargement of the phase diagram in the microcanonical ensemble.

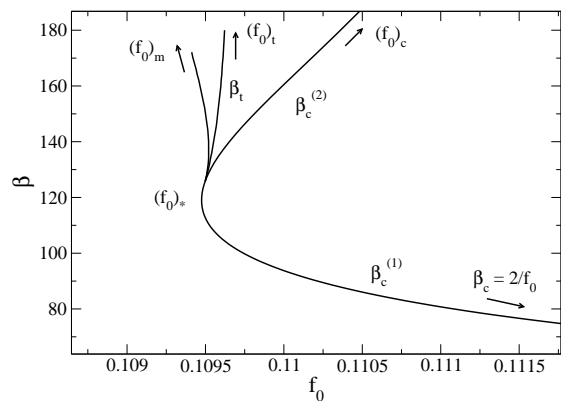


FIG. 3: Phase diagram in the canonical ensemble.

#### B. Region 5

In Figs. 5-7 we plot the series of equilibria in Region 5 corresponding to  $f_0 > (f_0)_c$  where  $(f_0)_c = 1/(2\pi\sqrt{2}) \simeq 0.11253954$  (see Fig. 1) [74, 81]. Specifically, we consider  $f_0 = 0.1130$ .

The homogeneous phase exists at any accessible energy. It is fully stable for  $E > E_c$  and unstable for  $E < E_c$ . The inhomogeneous phase exists for  $E < E_c$ . It has a higher entropy (see Fig. 6) than the homogeneous phase and it is fully stable. Therefore, the microcanonical caloric curve displays a second order phase transition between homogeneous and inhomogeneous states marked by the discontinuity of  $\beta'(E)$  at  $E = E_c$ . In the entropic curve of Fig. 6, this corresponds to a discontinuity of the second derivative  $S''(E) = \beta'(E)$  at  $E = E_c$ . The magnetization passes from  $M = 0$  for  $E > E_c$  to  $M \neq 0$  for  $E < E_c$  but remains continuous at the transition (see Fig. 7). The discussion is similar in the canonical ensemble.

Region 5: (i) in the MCE, there exists a second order phase transition at  $E_c$ . (ii) In the CE, there exists a second order phase transition at  $\beta_c$ . The ensembles are

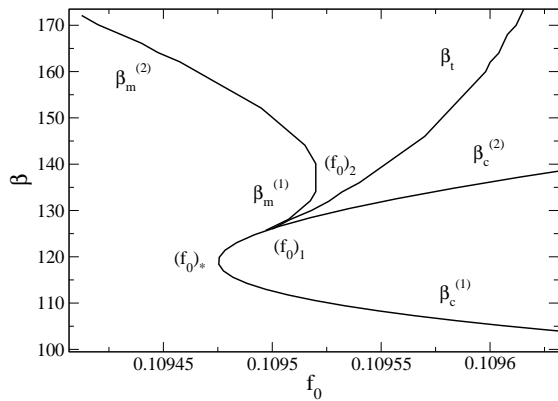


FIG. 4: Enlargement of the phase diagram in the canonical ensemble.

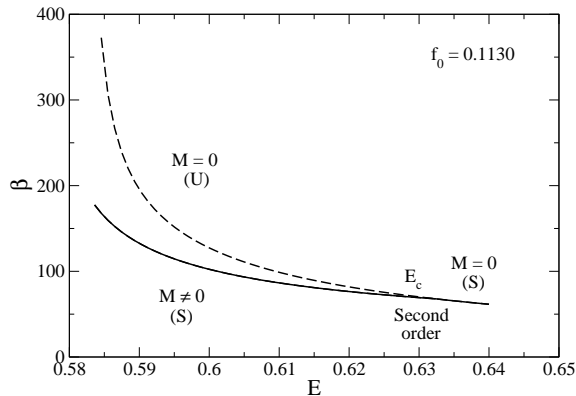


FIG. 5: Series of equilibria in Region 5 displaying microcanonical and canonical second order phase transitions at  $E_c$  and  $\beta_c$  respectively.

equivalent.

### C. Region 4

In Figs. 8-10 we plot the series of equilibria in Region 4 corresponding to  $(f_0)_t < f_0 < (f_0)_c$  where  $(f_0)_t \simeq 0.10965$  and  $(f_0)_c \simeq 0.11253954$  (see Fig. 1). Specifically, we consider  $f_0 = 0.1110$ .

The homogeneous phase exists at any accessible energy. It is fully stable for  $E > E_c^{(1)}$ , unstable for  $E_c^{(2)} < E < E_c^{(1)}$  and metastable for  $E < E_c^{(2)}$ . A first inhomogeneous phase exists for  $E < E_c^{(1)}$ . It has a higher entropy than the homogeneous phase and it is fully stable (see Fig. 9). Therefore, the microcanonical caloric curve displays a second order phase transition between homogeneous and inhomogeneous states marked by the discontinuity of  $S''(E) = \beta'(E)$  at  $E = E_c^{(1)}$ . The magnetization passes from  $M = 0$  for  $E > E_c^{(1)}$  to  $M \neq 0$  for  $E < E_c^{(1)}$  but remains continuous at the transition

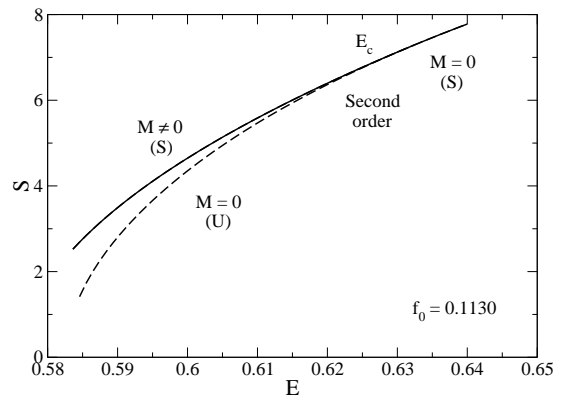


FIG. 6: Entropy versus energy in Region 5.

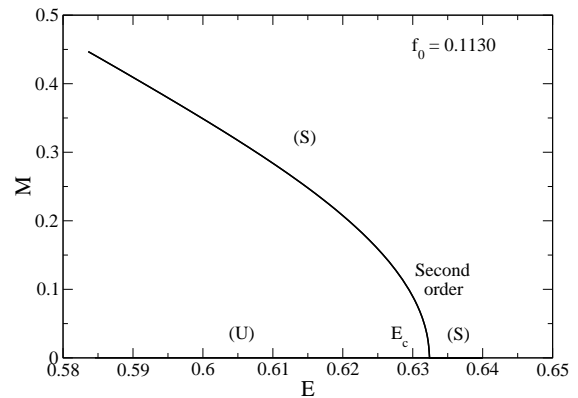


FIG. 7: Magnetization versus energy in Region 5.

(see Fig. 10). A second inhomogeneous phase exists for  $E < E_c^{(2)}$ . It appears precisely at the energy  $E_c^{(2)}$  at which the homogeneous phase becomes metastable. It has a lower entropy  $S$  than the homogeneous phase and the first inhomogeneous phase (see Fig. 9) and it is unstable. This branch is clearly visible on the magnetization curve (see Fig. 10). The discussion is similar in the canonical ensemble.

Region 4: (i) in the MCE, there exists a second order phase transition at  $E_c^{(1)}$ . (ii) In the CE, there exists a second order phase transition at  $\beta_c^{(1)}$ . The ensembles are equivalent.

### D. Region 3-c

In Figs. 11-16, we plot the series of equilibria in Region 3-c corresponding to  $(f_0)_2 < f_0 < (f_0)_t$  where  $(f_0)_2 \simeq 0.109519$  and  $(f_0)_t \simeq 0.10965$  (see Fig. 2). Specifically, we consider  $f_0 = 0.10963$ .

The homogeneous phase exists at any accessible energy. It is fully stable for  $E > E_c^{(1)}$ , unstable for  $E_c^{(2)} < E < E_c^{(1)}$ , metastable for  $E_t < E < E_c^{(2)}$  and

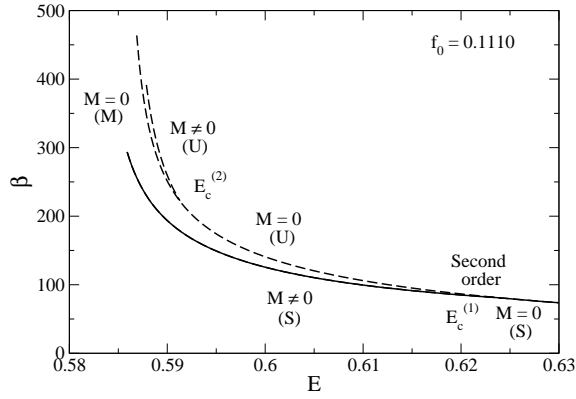


FIG. 8: Series of equilibria in Region 4 displaying microcanonical and canonical second order phase transitions at  $E_c^{(1)}$  and  $\beta_c^{(1)}$  respectively. At  $E_c^{(2)}$  and  $\beta_c^{(2)}$ , a second inhomogeneous phase appears (but is unstable) while the homogeneous phase becomes metastable.

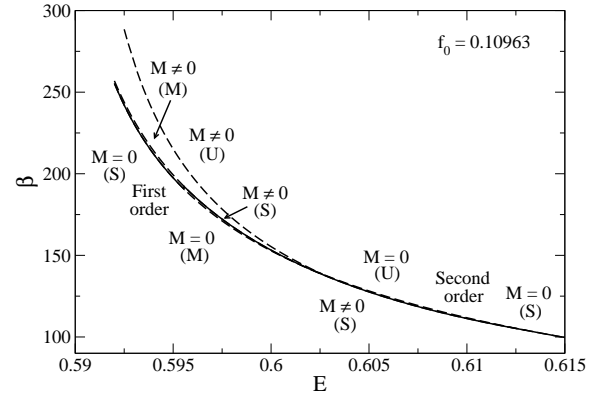


FIG. 11: Series of equilibria in Region 3-c. It displays microcanonical and canonical second order phase transitions at  $E_c^{(1)}$  and  $\beta_c^{(1)}$  respectively. It also displays microcanonical and canonical first order phase transitions at  $E_t$  and  $\beta_t$  respectively.

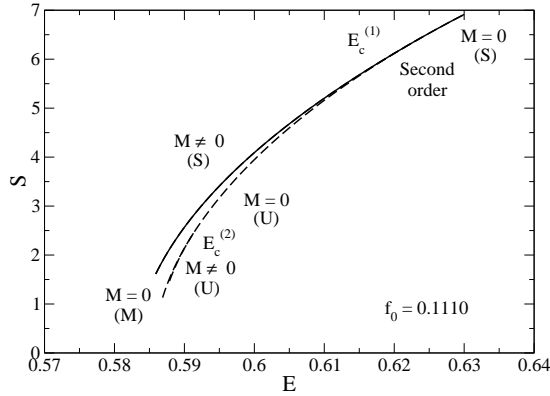


FIG. 9: Entropy versus energy in Region 4.

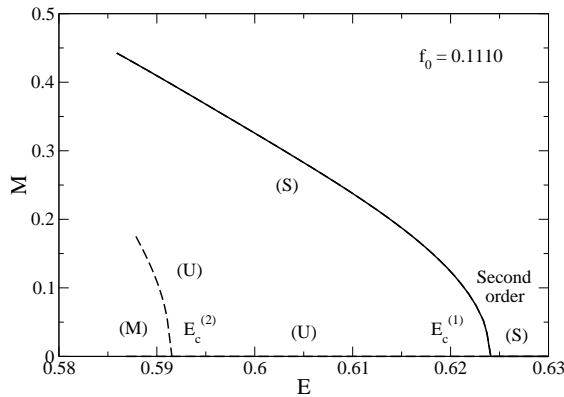


FIG. 10: Magnetization versus energy in Region 4. The unstable inhomogeneous phase is clearly visible.

fully stable for  $E < E_t$ . A first inhomogeneous phase exists for  $E < E_c^{(1)}$ . It is fully stable for  $E_t < E < E_c^{(1)}$  and metastable for  $E < E_t$ . Indeed, it has a higher entropy than the homogeneous phase for  $E_t < E < E_c^{(1)}$  and a lower entropy for  $E < E_t$ . Therefore, the microcanonical caloric curve displays a second order phase transition between homogeneous and inhomogeneous states marked by the discontinuity of  $\beta'(E) = S''(E)$  at  $E = E_c^{(1)}$  (see Fig. 12) and a first order phase transition between homogeneous and inhomogeneous states marked by the discontinuity of  $\beta(E) = S'(E)$  at  $E = E_t$  (see Fig. 14). The magnetization of the fully stable branch passes from  $M = 0$  to  $M \neq 0$  at  $E = E_c^{(1)}$  but remains continuous, and it passes from  $M \neq 0$  to  $M = 0$  at  $E = E_t$  by being discontinuous (see Fig. 16). We note that the first order phase transition is hardly visible on the caloric curve  $\beta(E)$  whereas it is clearly visible on the magnetization curve  $M(E)$ . A second inhomogeneous phase exists for  $E < E_c^{(2)}$ . It appears precisely at the energy  $E_c^{(2)}$  at which the homogeneous phase becomes metastable. It has a lower entropy  $S$  than the homogeneous phase and the first inhomogeneous phase and it is unstable. This branch is clearly visible on the magnetization curve of Fig. 16. The discussion is similar in the canonical ensemble.

Region 3-c: (i) In MCE, there exists a second order phase transition at  $E_c^{(1)}$  and a first order phase transition at  $E_t$  [96]. (ii) In CE, there exists a second order phase transition at  $\beta_c^{(1)}$  and a first order phase transition at  $\beta_t$ . For  $0.595477 \leq E \leq 0.595629$ , the ensembles are inequivalent (see Fig. 15). However, this concerns a strikingly narrow range of energies.



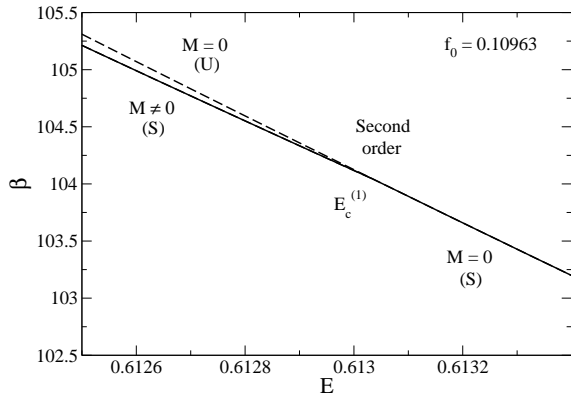


FIG. 12: Enlargement of Fig. 11 in the region of second order phase transition.

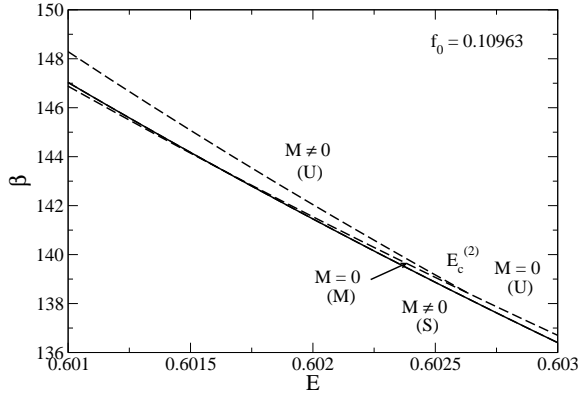


FIG. 13: Enlargement of Fig. 11 near the energy  $E_c^{(2)}$  where a second inhomogeneous phase (unstable) appears. At that point, the homogeneous phase becomes metastable. We also note, in passing, that the temperatures of the metastable homogeneous phase and of the fully stable inhomogeneous phase cross each other at some point but this does not signal a change of stability. In particular, the homogeneous phase remains metastable until the energy  $E_t$  of first order phase transition (see Fig. 14).

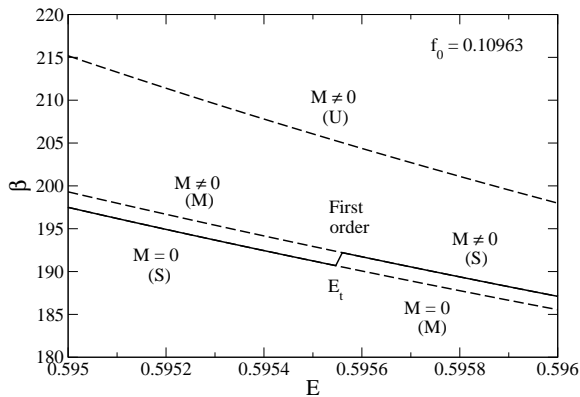


FIG. 14: Enlargement of Fig. 11 in the region of first order phase transition.

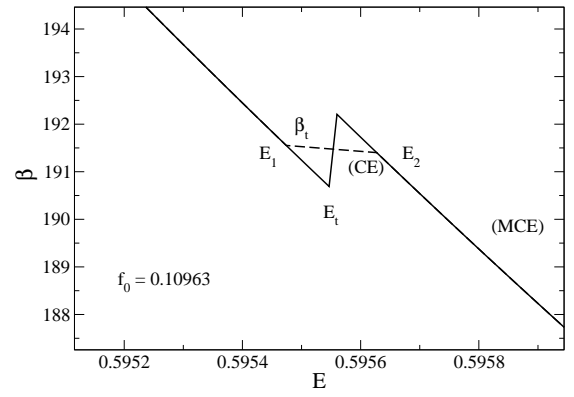


FIG. 15: Enlargement of Fig. 11 in the region of ensembles inequivalence. The full line corresponds to the strict caloric curve in the MCE and the dashed line to the strict caloric curve in the CE. The states between  $E_1 \simeq 0.59547$  and  $E_2 \simeq 0.595629$  are stable in the microcanonical ensemble while they are unstable (i.e. inaccessible) in the canonical ensemble. Note that the domain of ensembles inequivalence is almost imperceptible.

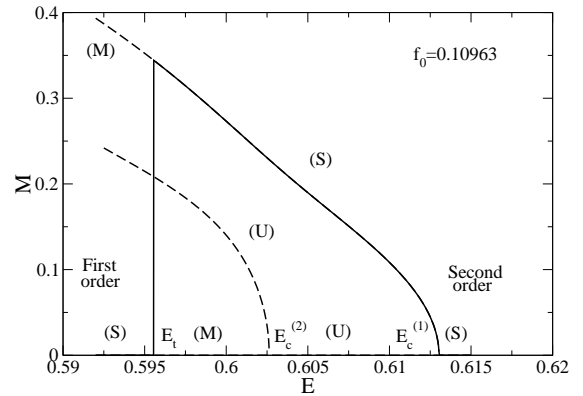


FIG. 16: Magnetization versus energy in Region 3-c showing clearly the first and second order phase transitions as well as the second (unstable) inhomogeneous branch.

### E. Region 3-b

In Figs. 17-21, we plot the series of equilibria in Region 3-b corresponding to  $(f_0)_1 < f_0 < (f_0)_2$  where  $(f_0)_1 \simeq 0.109497$  and  $(f_0)_2 \simeq 0.109519$  (see Fig. 2). Specifically, we consider  $f_0 = 0.10950$ .

The homogeneous phase exists at any accessible energy. It is fully stable for  $E > E_c^{(1)}$ , unstable for  $E_c^{(2)} < E < E_c^{(1)}$ , metastable for  $E_t < E < E_c^{(2)}$  and fully stable for  $E < E_t$ . A first inhomogeneous phase exists for  $E_m^{(1)} < E < E_c^{(1)}$  and  $E < E_m^{(2)}$  (it does not exist between  $E_m^{(2)}$  and  $E_m^{(1)}$ ). It is fully stable for  $E_t < E < E_c^{(1)}$  and metastable for  $E_m^{(1)} < E < E_t$  and for  $E < E_m^{(2)}$ . Therefore, the microcanonical caloric

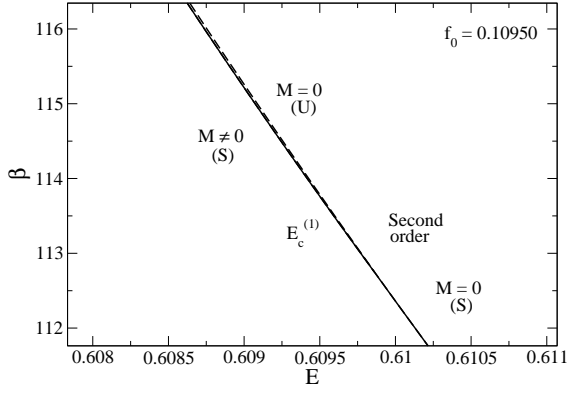


FIG. 17: Series of equilibria in Region 3-b near the point of second order phase transition.

curve displays a second order phase transition between homogeneous and inhomogeneous states marked by the discontinuity of  $\beta'(E) = S''(E)$  at  $E = E_c^{(1)}$  and a first order phase transition between homogeneous and inhomogeneous states marked by the discontinuity of  $\beta(E) = S'(E)$  at  $E = E_t$ . A second inhomogeneous phase exists for  $E_m^{(1)} < E < E_c^{(2)}$  and for  $E < E_m^{(2)}$  (it does not exist between  $E_m^{(2)}$  and  $E_m^{(1)}$ ). It appears precisely at the energy  $E_c^{(2)}$  at which the homogeneous phase becomes metastable. This second inhomogeneous phase is always unstable. The first and second order phase transitions are better visible on the magnetization curves of Figs. 20 and 21. The discussion is similar in the canonical ensemble.

Region 3-b: (i) In MCE, there exists a second order phase transition at  $E_c^{(1)}$  and a first order phase transition at  $E_t$ . (ii) In CE, there exists a second order phase transition at  $\beta_c^{(1)}$  and a first order phase transition at  $\beta_t$ . As in region 3-c, there exists a tiny region of ensembles inequivalence.

### F. Region 3-a

In Figs. 22-24, we plot the series of equilibria in Region 3-a corresponding to  $(f_0)_* < f_0 < (f_0)_1$  where  $(f_0)_* \simeq 0.10947$  and  $(f_0)_1 \simeq 0.109497$  (see Fig. 2). Specifically, we consider  $f_0 = 0.109480$ .

The homogeneous phase exists at any accessible energy. It is fully stable for  $E > E_c^{(1)}$ , unstable for  $E_c^{(2)} < E < E_c^{(1)}$ , and fully stable for  $E < E_c^{(2)}$ . A first inhomogeneous phase exists for  $E_c^{(2)} < E < E_c^{(1)}$  and for  $E < E_m^{(2)}$  (it does not exist for  $E_m^{(2)} < E < E_c^{(2)}$ ). It is fully stable for  $E_c^{(2)} < E < E_c^{(1)}$  and metastable for  $E < E_m^{(2)}$ . Therefore, the microcanonical caloric curve displays two second order phase transitions between homogeneous and inhomogeneous states marked by the dis-

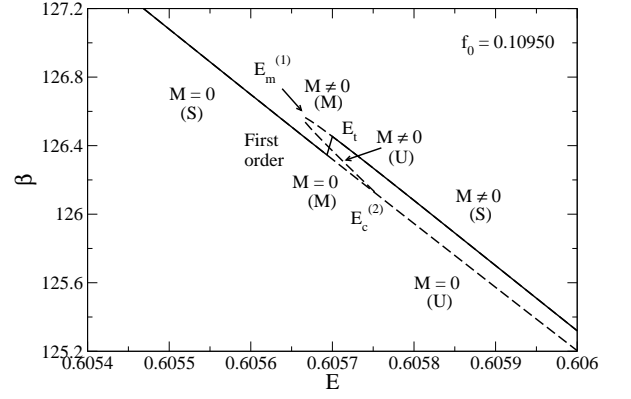


FIG. 18: Series of equilibria in Region 3-b near the point of first order phase transition. We also see the disappearance of the inhomogeneous phases for  $E < E_m^{(1)}$ . In particular, the energy  $E_m^{(1)}$  can be interpreted as a spinodal point at which the inhomogeneous metastable branch disappears.

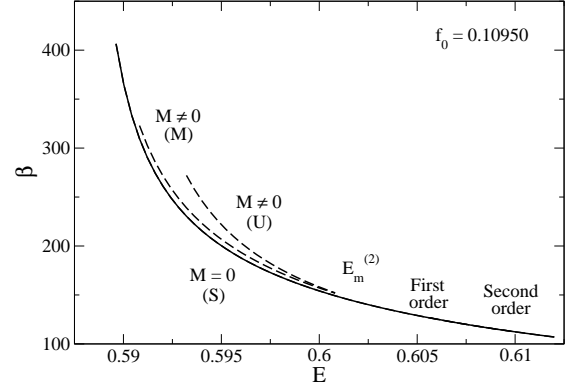


FIG. 19: Series of equilibria in Region 3-b. We see the reappearance of the inhomogeneous phases for  $E < E_m^{(2)}$ . The energy  $E_m^{(2)}$  can also be interpreted as a spinodal point.

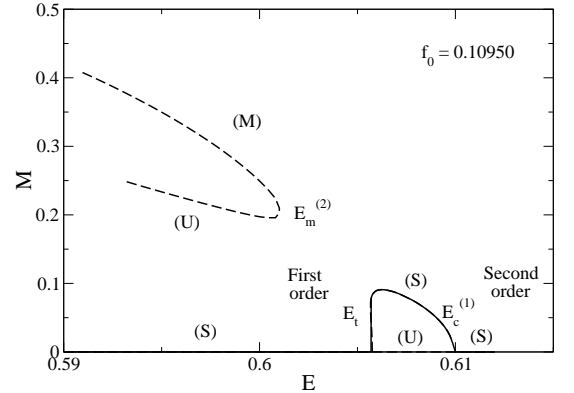


FIG. 20: Magnetization versus energy in Region 3-b.

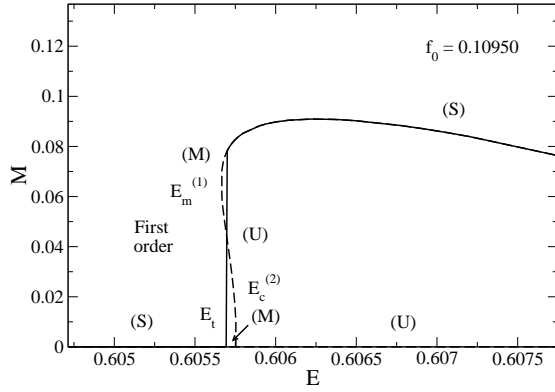


FIG. 21: Enlargement of Fig. 20 in the region of first order phase transition.

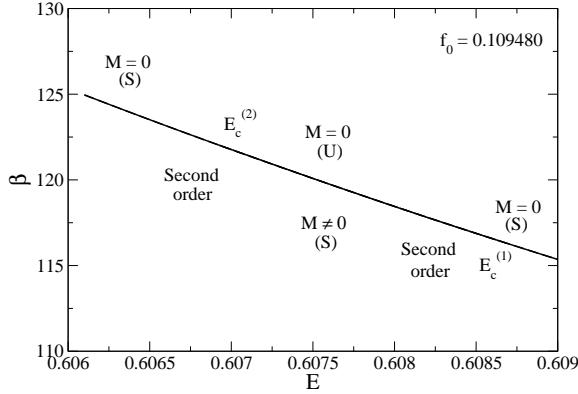


FIG. 22: Series of equilibria in Region 3-a. It displays two microcanonical and canonical second order phase transitions at  $E_c^{(1)}$ ,  $E_c^{(2)}$  and at  $\beta_c^{(1)}$ ,  $\beta_c^{(2)}$  respectively.

continuity of  $\beta'(E) = S''(E)$  at  $E = E_c^{(1)}$  and  $E = E_c^{(2)}$ . The magnetization of the fully stable branch passes from  $M = 0$  to  $M \neq 0$  at  $E = E_c^{(1)}$  and from  $M \neq 0$  to  $M = 0$  at  $E = E_c^{(2)}$ , but remains continuous at the transition (see Fig. 23). We note that the second order phase transitions are hardly visible on the caloric curve  $\beta(E)$  whereas they are clearly visible on the magnetization curve  $M(E)$ . A second inhomogeneous phase exists for  $E < E_m^{(2)}$  and it is unstable. The discussion is similar in the canonical ensemble.

Region 3-a: (i) In MCE, there exists two second order phase transitions at  $E_c^{(1)}$  and  $E_c^{(2)}$ ; (ii) in CE, there exists two second order phase transitions at  $\beta_c^{(1)}$  and  $\beta_c^{(2)}$ . The ensembles are equivalent.

### G. Region 2

In Figs. 25-27, we plot the series of equilibria in Region 2 corresponding to  $(f_0)_m < f_0 < (f_0)_*$  where  $(f_0)_m \simeq$

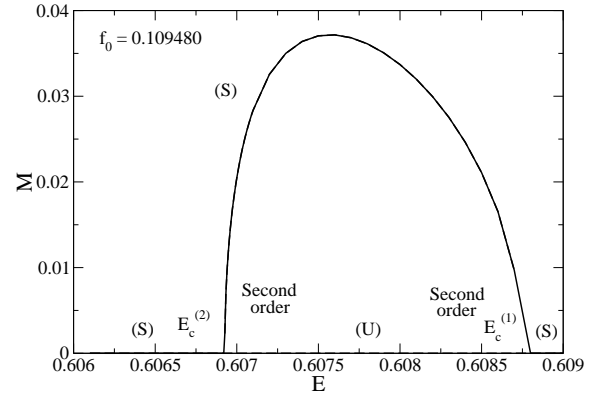


FIG. 23: Magnetization versus energy in Region 3-a. It displays two microcanonical second order phase transitions at  $E_c^{(1)}$  and  $E_c^{(2)}$ .

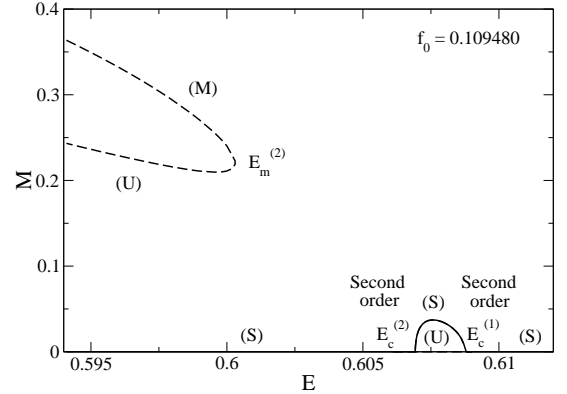


FIG. 24: Extension of Fig. 23 showing the reappearance of the inhomogeneous phase for  $E < E_m^{(2)}$ .

0.1075 and  $(f_0)_* \simeq 0.10947$  (see Fig. 1). Specifically, we consider  $f_0 = 0.10900$ .

The homogeneous phase exists at any accessible energy and it is fully stable. Therefore, the microcanonical caloric curve does not display any phase transition and is made of homogeneous states. Two inhomogeneous phases appear for  $E < E_m$ , one being metastable and the other unstable. The metastable phase has a lower entropy than the homogeneous phase and the unstable phase has a lower entropy than the metastable phase (see Fig. 26). These different phases can also be seen on the magnetization (order parameter) curve of Fig. 27. The discussion is similar in the canonical ensemble.

Region 2: There is no phase transition and the ensembles are equivalent.

### H. Region 1

In Figs. 28 and 29, we plot the series of equilibria in Region 1 corresponding to  $f_0 < (f_0)_m$  where

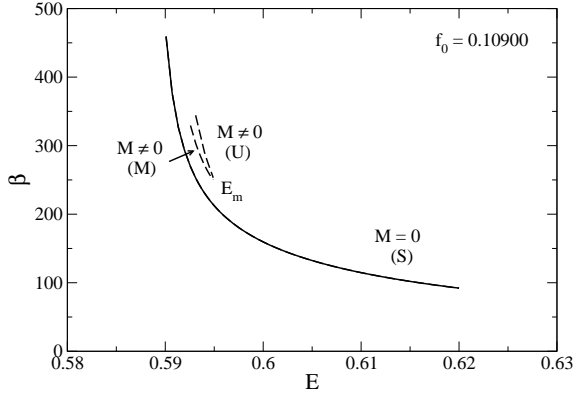


FIG. 25: Series of equilibria in Region 2. There is no phase transition but the sudden appearance of a metastable inhomogeneous branch, accompanied by an unstable inhomogeneous branch, at  $E = E_m$ .

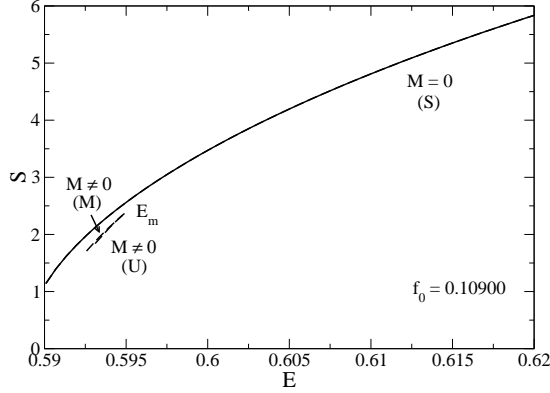


FIG. 26: Entropy versus energy in Region 2.

$(f_0)_m \simeq 0.1075$  (see Fig. 1). Specifically, we consider  $f_0 = 0.10600$ .

The homogeneous phase exists at any accessible energy and it is fully stable. There is no inhomogeneous phase. Therefore, the microcanonical caloric curve does not display any phase transition and is made of homogeneous states (see Figs. 28 and 29). The discussion is similar in the canonical ensemble.

Region 1: There is no phase transition and the ensembles are equivalent.

#### IV. DISCUSSION

Let us summarize the different results obtained in the previous analysis:

(i) Decreasing  $f_0$ , the system successively exhibits one second order phase transition (Regions 5 and 4), one second order and one first order phase transition (Regions 3-c and 3-b), two second order phase transitions (Region 3-a), and no phase transition (Regions 2 and 1).

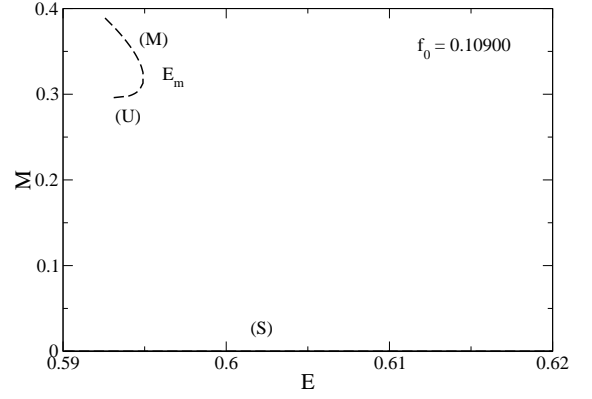


FIG. 27: Magnetization versus energy in Region 2.

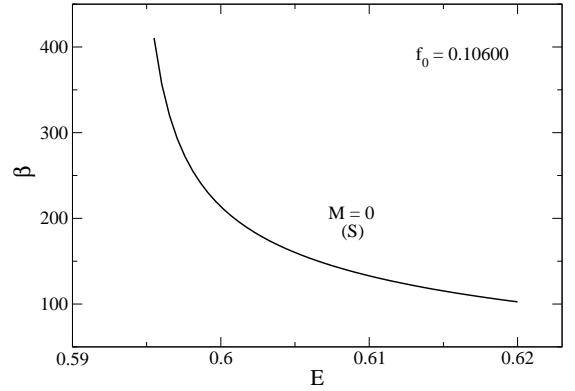


FIG. 28: Series of equilibria in Region 1.

(ii) There exists a *tricritical point* corresponding to the passage from a first order phase transition to a second order phase transition. It is located at  $((f_0)_1, E_1, \beta_1) \simeq (0.109497, 0.6059, 125)$ .

(iii) The sudden appearance of two second order phase transitions at the turning point  $((f_0)_*, E_*, \beta_*) \simeq$

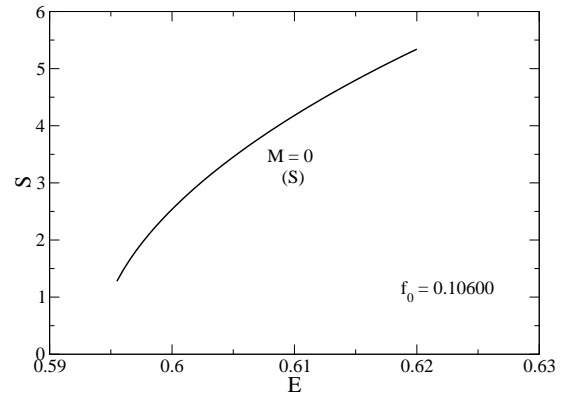


FIG. 29: Entropy versus energy curve in Region 1.

(0.10947, 0.608, 118) is sometimes called *second order azeotropy* [27].

(iv) For  $(f_0)_* < f_0 < (f_0)_c$ , there is a phenomenon of *phase reentrance* concerning the homogeneous phase [74, 81]. As we reduce the energy, the homogeneous phase is successively stable, unstable and stable (or metastable) again. This phenomenon is basically due to the turning point of the energy curve  $E_c(f_0)$  at  $f_0 = (f_0)_*$ . It is therefore associated with the second order azeotropy.

(v) For  $(f_0)_* < f_0 < (f_0)_2$ , there is a phenomenon of phase reentrance concerning the inhomogeneous phase. As we reduce the energy, the inhomogeneous phase is stable (or metastable), then it disappears, and it finally reappears as a metastable state. This phenomenon is basically due to the turning point of the energy curve  $E_m(f_0)$  at  $f_0 = (f_0)_2$ . It is located at  $((f_0)_2, E_2, \beta_2) \simeq (0.109519, 0.603, 137)$ .

(vi) The tricritical point  $((f_0)_1, E_1)$  separating first and second order phase transitions is located between the turning points of the  $E_c(f_0)$  and  $E_m(f_0)$  curves.

(vii) In Regions 3-c and 3-b, there is a very small zone of ensembles inequivalence associated with the first order phase transitions.

In conclusion, the out-of-equilibrium phase transitions of the HMF model predicted by the Lynden-Bell theory lead to a rich and interesting phase diagram. It is striking that everything happens in a very narrow range of parameters  $(f_0)_m \simeq 0.1075 < f_0 < (f_0)_c \simeq 0.11253954$ , although  $f_0$  can take in principle all positive values. A similar observation has been made previously in other studies of phase transitions in systems with long-range interactions [77, 84–86]. The branches corresponding to the different phases are very close to each other in the series of equilibria  $\beta(E)$  and in the entropic curves  $S(E)$ . This shows in particular that all the phases have almost the same entropy, even the unstable ones. However, the branches appear to be well separated in the kinetic caloric curve  $\beta_{kin}(E)$  [82] and in the magnetization curve  $M(E)$ .

## V. NUMERICAL SIMULATIONS

The numerical results obtained in [81] show that the phase diagram deduced from the Lynden-Bell theory predicts the right phenomenology, even in the small and quite complex region located around the tricritical point. In this section, we show that, in the region of metastability (according to Lynden-Bell’s theory), the system displays the usual dynamical behavior of systems in a metastable state: a “lethargic” evolution during which the system is trapped in a given macrostate (metastable), followed by a sudden jump in a different macrostate (fully stable). To the best of our knowledge, this is the first evidence of metastability during a QSS. Our results are obtained from a set of molecular dynamics simulations carried out after having prepared the system in a state belonging to the region of the  $(f_0, E)$  plane close to the first order transition line. For the chosen param-

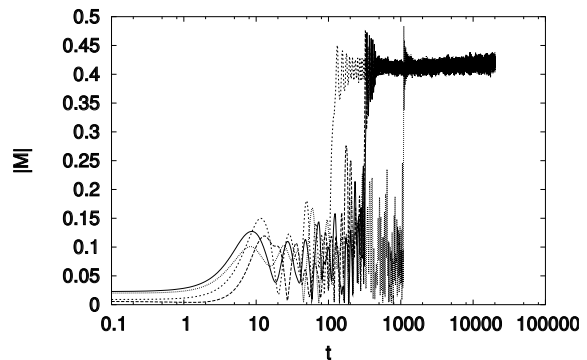


FIG. 30: Magnetization as a function of time for a system of  $N = 20000$  particles at energy  $E = 0.5901$ . The four curves are different realizations of the same initial distribution with  $f_0 = 0.1097$ . The initial condition is a rectangular waterbag distribution with magnetization  $M_0 \simeq 0.01413$  (see Eq. (28) of [81]).

eters  $(f_0, E) = (0.1097, 0.5901)$ , the homogeneous phase is metastable and the inhomogeneous phase is fully stable (see Fig. 1). Following the temporal evolution of the magnetization (see Fig. 30), one first observes the spontaneous relaxation of the system in the unmagnetized phase (metastable), followed by a sudden jump in the magnetized state (fully stable).

Different runs with the same initial distribution show that the jump occurs at random times. This is in agreement with the ordinary behavior of metastable states, where the time of the jump depends on the particular “realization”. The average time at which the jump occurs depends on the size of the system and increases with  $N$ . This indicates that “collisions” (finite  $N$  effects) play some role in the dynamics. This is relatively unexpected since the regime that we are exploring corresponds to the QSS regime where the Vlasov equation should be applicable. In all the numerical simulations that we have run, the system spontaneously relaxes towards the metastable state; it never directly reaches the fully stable state. The selection of the QSS, among these two states, obviously depends on a complicated notion of *basin of attraction*. Our initial condition consists in a rectangular waterbag distribution which has a very small magnetization  $M_0 \simeq 0.01744$  since the chosen energy is close to the minimum energy state  $E_{min}(f_0) \simeq 0.58766$  which is a waterbag distribution with vanishing magnetization [74, 81]. It is likely that this initial condition belongs to the basin of attraction of the homogeneous metastable state. It is possible that changing the initial condition (still with two levels and with the same  $f_0$  and  $E$  but no more waterbag) so as to increase the magnetization  $M_0$  may help the system to access directly to the inhomogeneous (fully stable) state. On the other hand, on the other side of the first order transition line (i.e. for smaller values of  $f_0$ ), the homogeneous state becomes fully stable while the inhomogeneous state is metastable.

In that case, starting from a rectangular waterbag initial condition, the system relaxes towards the homogeneous state (since it belongs to its basin of attraction) and stays there during the whole QSS regime since it is now fully stable (numerical simulations not shown). Additional numerical simulations are necessary to get a more general picture of the QSS metastability for different values of the control parameters  $(f_0, E)$  and different types of initial conditions.

## VI. CONCLUSION

In this paper we have explored the phase diagram obtained by applying Lynden-Bell’s statistical theory to the HMF model. We have found a richer phenomenology in the  $(f_0, E)$  plane [74, 81] than in the  $(M_0, E)$  plane [78, 79]. We have also explained that the proper external parameter to use in the Lynden-Bell theory is  $f_0$ , not  $M_0$ . The choice of the proper control parameters has deep consequences on the thermodynamical analysis.

The HMF model is a system in which the Lynden-Bell theory works relatively well (in contrast to astrophysical systems for which it was initially devised [29]). In particular, the phenomenon of phase reentrance that is predicted on the basis of this theory [74] has been successfully reproduced in [81]. Numerical evidence of first and second order phase transitions has also been given in [81] in agreement with theory [97]. This is remarkable because all these interesting features occur in a very small region of the phase diagram (typically  $(f_0)_m \simeq 0.1075 < f_0 < (f_0)_c \simeq 0.11253954$ ). In this sense, the Lynden-Bell prediction is not only qualitative but in fact extremely accurate!

There are, however, cases where the Lynden-Bell theory fails. In the numerical study of [81], some discrepancies with the Lynden-Bell prediction were reported. In particular, unmagnetized states are observed in the *a priori* magnetized region leading to a second reentrant phase. Inversely, magnetized states are observed in the *a priori* unmagnetized region. On the other hand, the Lynden-Bell theory cannot explain the region of negative kinetic specific heat observed numerically by Antoni & Ruffo [32] and Latora *et al.* [70]. These authors start from an initial condition with magnetization  $M_0 = 1$  in which all the particles are located at  $\theta = 0$ . The initial distribution function  $f_0$  is infinite corresponding to the dilute (or non degenerate) limit of the Lynden-Bell theory in which the predicted QSS coincides with the Boltzmann distribution. Now, the results of numerical simulations [32, 70] are inconsistent with the Boltzmann (hence Lynden-Bell) distribution in the region of negative kinetic specific heats. This means that violent relaxation is incomplete [30] and that the system is trapped in a stable steady state of the Vlasov equation that is not the most mixed (i.e. Lynden-Bell) state [74]. Recently, Chavanis & Campa [77] have investigated the Vlasov dynamical stability of polytropic (or Tsallis) distributions

and argued that polytropes with an index close to  $n = 1$  could provide an explanation of the curious anomalies observed in [32, 70]. In this work, the polytropic distributions are justified by a lack of ergodicity and by incomplete relaxation. It would be interesting to extend their analysis (restricted so far to initial conditions with magnetization  $M_0 = 1$ ) so as to cover a wider range of parameters and see whether it can explain similarly the anomalies reported in [81].

Very recently, a mathematical “tour de force” has been accomplished by Mouhot & Villani [87] who rigorously proved that systems with long-range interactions described by the Vlasov equation possess some asymptotic “stabilization” property in large time, although the Vlasov equation is time-reversible. More precisely, they show that if a stable steady state of the Vlasov equation is slightly perturbed, the perturbation converges in a *weak sense* towards a steady distribution through phase mixing without the help of any extra diffusion or ensemble averaging. This is referred to as *nonlinear Landau damping*. This is a very important work that shades new light on the process of phase mixing and, consequently, on the nature of QSSs. However, these authors criticize the Lynden-Bell approach arguing that there is no “universal” large time behavior of the solutions of the Vlasov equation in terms of just the conservation laws and the initial datum. In their words: “This seems to be bad news for the statistical theory of the Vlasov equation pioneered by Lynden-Bell”. Although it is clear that the Lynden-Bell theory has some limitations due to incomplete relaxation (lack of mixing/ergodicity) [30], our series of works related to the HMF model [74, 81, 82], including the present effort, shows that the Lynden-Bell approach is able to make accurate predictions that are confirmed by direct numerical simulations. Therefore, the Lynden-Bell theory remains a valuable tool even if it is difficult to specify its general domain of validity. In fact, Mouhot & Villani [87] do not totally reject this statistical approach and point out limitations in the application of their results. In particular, their theory is based on smooth functions (which is not the norm in statistical theories) and Landau damping is a thin effect which might be neglected when it comes to predict the “final” state in a “turbulent” situation (which is precisely the aim of Lynden-Bell’s statistical theory). The subject is certainly not closed and should lead again to interesting findings and fruitful discussions.

## Appendix A: The ground state

In this Appendix, we briefly discuss the ground state of the Lynden-Bell distribution (analogous to the Fermi-Dirac distribution) and its connection with the phase diagram of Fig. 1.

For a given value of  $f_0$ , the minimum energy state corresponds to a Fermi distribution at  $T = 0$ , i.e. a (possibly spatially inhomogeneous) waterbag distribution. Such a

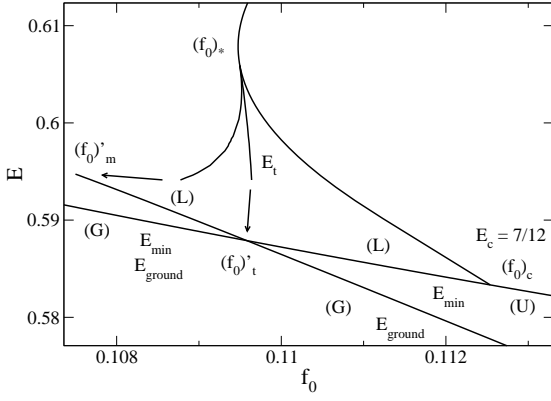


FIG. 31: Phase diagram close to the ground state. The upper full lines correspond to states that have been actually computed. Arrows give the directions towards which these branches should tend. The lower line denoted  $E_{min}$  (like in Fig. 1) corresponds to the spatially homogeneous waterbag distribution as explained in [74, 81]. Its energy is  $E_{min} = 1/(96\pi^2 f_0^2) + 1/2$ . It is the global energy minimum for  $f_0 < (f_0)'_t$ , a local energy minimum for  $(f_0)'_t < f_0 < (f_0)_c$  and an unstable saddle point for  $f_0 > (f_0)_c$ . The other lower line corresponds to the inhomogeneous waterbag distribution as explained in [88]. It starts at  $f_0 = (f_0)'_m$  (corresponding to an energy  $E'_m \simeq 0.59473$ ) and tends to  $E = 0$  for  $f_0 \rightarrow +\infty$ . It is a local energy minimum for  $(f_0)'_m < f_0 < (f_0)'_t$  and a global energy minimum for  $f_0 > (f_0)'_t$ . The unstable inhomogeneous waterbag distribution has not been represented (see [88] for details).

distribution is equivalent to a polytrope of index  $n = 1/2$  [77]. Its structure and stability are described in detail in [77, 88]. Here, we only give the final results of the analysis (see Figs. 31 and 32) and refer the reader to [77, 88] for more details. The global minimum energy state (G) is a spatially homogeneous waterbag distribution for  $f_0 < (f_0)'_t \simeq 0.109579$  and a spatially inhomogeneous waterbag distribution for  $f_0 > (f_0)'_t$ . On the other hand, the spatially inhomogeneous waterbag distribution is a local minimum energy state (L) for  $(f_0)'_m \simeq 0.1075 < f_0 < (f_0)'_t$  and the spatially homogeneous waterbag distribution is a local minimum energy state (L) for  $(f_0)'_t < f_0 < (f_0)_c = 1/(2\pi\sqrt{2})$ . For  $f_0 < (f_0)'_m$  (spinodal point), no spatially inhomogeneous waterbag distribution exists and for  $f_0 > (f_0)_c$  the spatially homogeneous waterbag distribution is an unstable saddle point of energy.

We emphasize that the specific form of the initial condition may constrain the accessible range of energies. For example, for a rectangular waterbag initial distribution, the minimum accessible energy  $E_{MIN}(f_0)$  is strictly larger than the ground state  $E_{ground}(f_0)$  for  $f_0 > (f_0)'_t$  (see Fig. 1). Of course, smaller energies can be achieved by other types of initial conditions.

It is likely that the point  $(f_0)'_t \simeq 0.109579$  should coincide with the transition point  $(f_0)_t$  in the phase diagram of Fig. 1 although we gave a different value  $(f_0)_t \simeq$

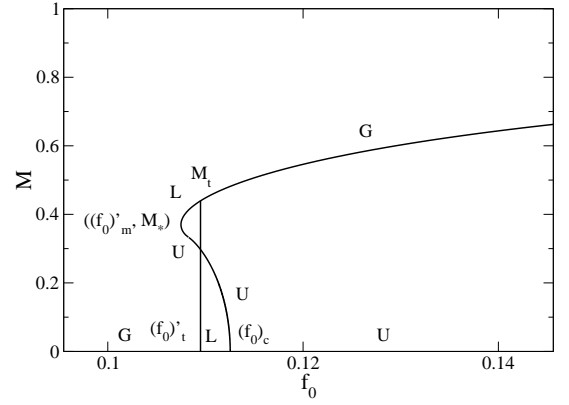


FIG. 32: Magnetization of the minimum energy state (ground state) as a function of the maximum value of the distribution  $f_0$  (taken from [88]). It exhibits a first order phase transition at  $(f_0)'_t$ . The homogeneous waterbag distribution is the global energy minimum for  $f_0 < (f_0)'_t$ , a local energy minimum for  $(f_0)'_t < f_0 < (f_0)_c$  and an unstable saddle point for  $f_0 > (f_0)_c$ . The inhomogeneous waterbag distribution exists only for  $f_0 > (f_0)'_m$ . It is a local energy minimum for  $(f_0)'_m < f_0 < (f_0)'_t$  (corresponding to  $M_* \simeq 0.37 < M < M_t \simeq 0.44$ ) and the global energy minimum for  $f_0 > (f_0)'_t$  (corresponding to  $M > M_t$ ). It is an unstable saddle point for  $(f_0)'_m < f_0 < (f_0)_c$  and  $M < M_*$ .

0.10965 in Sec. III. In fact, as we indicated in the caption of Fig. 1, the curve  $E_t(f_0)$  has been continued “by hand” for small energies so that the value  $(f_0)_t \simeq 0.10965$  is not firmly established and may be incorrect. The points that have been actually computed are shown in Fig. 31. It is likely that the real curve  $E_t(f_0)$  tends to the point  $((f_0)'_t, E_t((f_0)'_t)) \simeq (0.109579, 0.587896)$ . If this picture is correct, it implies that the curve  $E_t(f_0)$  is multivalued in some range of parameters  $[(f_0)'_t, (f_0)_{new}]$  (say). Indeed, some of the computed points have values of  $f_0$  larger than  $(f_0)'_t$  so that the curve must turn back. This yields an even more complex phase diagram with an additional phase reentrance. Indeed, decreasing the energy in the range  $[(f_0)'_t, (f_0)_{new}]$ , the homogeneous phase is successively stable, unstable, metastable, stable, and metastable again. On the other hand, the inhomogeneous phase is inexistent, stable, metastable and stable again. There exists therefore one second order phase transition and two first order phase transitions in this range of parameters.

On the other hand, it is likely that the local minimum energy state for  $(f_0)'_m < f_0 < (f_0)'_t$  corresponds to the minimum accessible energy of the inhomogeneous phase while the local minimum energy state for  $(f_0)'_t < f_0 < (f_0)_c$  corresponds to the minimum accessible energy of the homogeneous phase. As a result, the curve  $E_m^{(2)}(f_0)$  would not connect the point  $((f_0)_m, E_m) \simeq (0.1075, 0.59133)$  as shown in Fig. 1 but rather the point  $((f_0)'_m, E'_m) \simeq (0.1075, 0.59473)$  as shown in Fig. 31.

Additional numerical simulations would be necessary

to ascertain these results but they need to be very accurate and we experienced numerical problems when ap-

proaching the minimum energy.

- 
- [1] Dynamics and Thermodynamics of Systems with Long-Range Interactions, edited by T. Dauxois, S. Ruffo, E. Arimondo and M. Wilkens, Lectures Notes in Physics **602** (Berlin: Springer, 2002)
- [2] Dynamics and Thermodynamics of Systems with Long-Range Interactions: Theory and Experiments, edited by A. Campa, A. Giansanti, G. Morigi and F. Sylos Labini, AIP Conf. Proc. **965** 122 (2008)
- [3] Long-Range Interacting Systems, edited by T. Dauxois, S. Ruffo and L. Cugliandolo, Les Houches Summer School 2008, (Oxford: Oxford University Press, 2009)
- [4] A. Campa, T. Dauxois, S. Ruffo, Physics Reports **480**, 57 (2009)
- [5] T. Padmanabhan, Phys. Rep. **188**, 287 (1990)
- [6] J. Katz, Found. Phys. **33**, 223 (2003)
- [7] P.H. Chavanis, Int. J. Mod. Phys. B, **20**, 3113 (2006)
- [8] P. Tabeling, Phys. Rep. **362**, 1 (2002)
- [9] J. Sommeria, Two-Dimensional Turbulence in New Trends in Turbulence, edited by M. Lesieur, A. Yaglom, F. David, Les Houches Summer School **74**, 385 (2001)
- [10] P.H. Chavanis, Statistical Mechanics of Two-Dimensional Vortices and Stellar Systems in [1]
- [11] J.D. Murray, Mathematical Biology (Springer, Berlin, 1991)
- [12] D.R. Nicholson, Introduction to Plasma Theory (Krieger Publishing Company, Florida, 1992)
- [13] R.C. Davidson, Physics of Nonneutral Plasmas (World Scientific, 2001).
- [14] D. Dubin, T. O'neil, Rev. Mod. Phys. **71**, 87 (1999)
- [15] W.B. Colson, C. Pellegrini and A. Ranieri (Eds.), Free-electron lasers, Laser Handbook. **Vol.6** (NorthHolland, Amsterdam, 1990)
- [16] H.P. Freund and T. M. Antonsen, Principles of free-electron lasers, (Chapman and Hall, 1992)
- [17] E.L. Saldin, E.V. Schneidmiller, M.V. Yurkov, The Physics of Free Electron Lasers (Springer, Verlag, 2000)
- [18] P.H. Chavanis, AIP Conf. Proc. **970**, 39 (2008)
- [19] F. Bouchet, S. Gupta, D. Mukamel, Physica A, **389**, 4389 (2010)
- [20] P.H. Chavanis, J. Stat. Mech., P05019 (2010)
- [21] J. Messer, H. Spohn, J. Stat. Phys. **29**, 561 (1982)
- [22] M. Kiessling, J. Stat. Phys. **55**, 203 (1989)
- [23] E. Caglioti, P.L. Lions, C. Marchioro, M. Pulvirenti, Commun. Math. Phys. **143**, 501 (1992)
- [24] R. Ellis, K. Haven, B. Turkington, J. Stat. Phys. **101**, 999 (2000)
- [25] Thirring, W.: Z. Phys. **235**, 339 (1970)
- [26] D. Lynden-Bell, R. Lynden-Bell, Mon. Not. R. Astron. Soc. **181**, 405 (1977)
- [27] F. Bouchet, J. Barré, J. Stat. Phys. **118**, 1073 (2005)
- [28] J. Binney, S. Tremaine, Galactic Dynamics (Princeton Series in Astrophysics, 1987)
- [29] D. Lynden-Bell, Mon. Not. R. Astron. Soc. **136**, 101 (1967)
- [30] P.H. Chavanis, Physica A **365**, 102 (2006)
- [31] S. Inagaki, T. Konishi, Publ. Astron. Soc. Jpn **45**, 733 (1993)
- [32] M. Antoni, S. Ruffo, Phys. Rev. E **52**, 2361 (1995)
- [33] S. Chandrasekhar, Principles of Stellar Dynamics (University of Chicago press, 1942)
- [34] G. Bertin, M. Stiavelli, A&A **137**, 26 (1984)
- [35] M. Stiavelli, G. Bertin, Mon. Not. R. Astron. Soc. **229**, 61 (1987)
- [36] J. Hjorth, J. Madsen, Mon. Not. R. Astron. Soc. **253**, 703 (1991)
- [37] M. Trenti, G. Bertin, T.S. van Albada, A&A **433**, 57 (2005)
- [38] Chavanis, P.H., Sommeria, J., Robert, R.: Astrophys. J. **471**, 385 (1996)
- [39] P.H. Chavanis, Mon. Not. R. Astron. Soc. **300**, 981 (1998)
- [40] P.H. Chavanis Physica A **387**, 1504 (2008)
- [41] P.H. Chavanis, J. Sommeria, Mon. Not. R. Astron. Soc. **296**, 569 (1998)
- [42] P.H. Chavanis, Phys. Rev. E **65**, 056123 (2002)
- [43] Y.Y. Yamaguchi, Phys. Rev. E **78**, 041114 (2008)
- [44] T.N. Teles, Y. Levin, R. Pakter, F. Rizzato, J. Stat. Mech, P05007 (2010)
- [45] P.H. Chavanis, Phys. Rev. E **69**, 066126 (2004)
- [46] I. Arad, D. Lynden-Bell, Mon. Not. R. Astron. Soc. **361**, 385 (2005)
- [47] J. Miller, Phys. Rev. Lett. **65**, 2137 (1990)
- [48] R. Robert, J. Sommeria, J. Fluid Mech. **229**, 291 (1991)
- [49] P.H. Chavanis, J. Stat. Mech., P05019 (2010)
- [50] X.P. Huang, C.F. Driscoll, Phys. Rev. Lett. **72**, 2187 (1994)
- [51] B. Boghosian, Phys. Rev. E **53**, 4754 (1996)
- [52] H. Brands, P.H. Chavanis, R. Pasmanter, J. Sommeria, Phys. Fluids **11**, 3465 (1999)
- [53] P.H. Chavanis, J. Sommeria, J. Fluid Mech. **314**, 267 (1996)
- [54] P.H. Chavanis, J. Sommeria, J. Fluid Mech. **356**, 259 (1998)
- [55] A. Venaille, F. Bouchet, Phys. Rev. Lett. **102**, 104501 (2009)
- [56] A. Naso, P.H. Chavanis, B. Dubrulle, Eur. Phys. J. B **77**, 187 (2010)
- [57] J.B. Taylor, M. Borchardt, P. Helander, Phys. Rev. Lett. **102**, 124505 (2009)
- [58] J. Sommeria, C. Staquet, R. Robert, J. Fluid Mech. **233**, 661 (1991)
- [59] P. Chen, M.C. Cross, Phys. Rev. E **54**, 6356 (1996)
- [60] N. Whitaker, B. Turkington, Phys. Fluids **6**, 3963 (1994)
- [61] B. Turkington, A. Majda, K. Haven, M. Dibattista, Proc. Natl. Acad. Sci. **98**, 12 346 (2001)
- [62] R. Ellis, K. Haven, B. Turkington, Nonlin. **15**, 239 (2002)
- [63] F. Bouchet, J. Sommeria, J. Fluid. Mech. **464**, 165 (2002)
- [64] P.H. Chavanis, J. Sommeria, Phys. Rev. E **65**, 026302 (2002)
- [65] A. Naso, P.H. Chavanis, B. Dubrulle, [arXiv:1007.0164]
- [66] R. Jordan, B. Turkington, J. Stat. Phys. **87**, 661 (1997)
- [67] N. Leprovost, B. Dubrulle, P.H. Chavanis, Phys. Rev. E **71**, 6311 (2005)
- [68] A. Naso, R. Monchaux, P.H. Chavanis, B. Dubrulle,



- Phys. Rev. E **81**, 066318 (2010)
- [69] P.H. Chavanis, J. Vatteville & F. Bouchet, Eur. Phys. J. B **46**, 61 (2005)
- [70] V. Latora, A. Rapisarda, C. Tsallis, Phys. Rev. E **64**, 056134 (2001)
- [71] C. Tsallis, J. Stat. Phys. **52**, 479 (1988)
- [72] Y. Yamaguchi, J. Barré, F. Bouchet, T. Dauxois, S. Ruffo, Physica A **337**, 36 (2004)
- [73] J. Barré, T. Dauxois, G. De Ninno, D. Fanelli, S. Ruffo, Phys. Rev. E **69**, 045501 (2004)
- [74] P.H. Chavanis, Eur. Phys. J. B **53**, 487 (2006)
- [75] A. Antoniazzi, D. Fanelli, J. Barré, P.H. Chavanis, T. Dauxois, S. Ruffo, Phys. Rev. E **75**, 011112 (2007)
- [76] A. Campa, A. Giansanti, G. Morelli, Phys. Rev. E **76**, 041117 (2007)
- [77] P.H. Chavanis, A. Campa, Eur. Phys. J. B **76**, 581 (2010)
- [78] A. Antoniazzi, D. Fanelli, S. Ruffo, Y. Yamaguchi, Phys. Rev. Lett. **99**, 040601 (2007)
- [79] A. Antoniazzi, F. Califano, D. Fanelli, S. Ruffo, Phys. Rev. Lett. **98**, 150602 (2007)
- [80] P.H. Chavanis, G. De Ninno, D. Fanelli, S. Ruffo, Out of equilibrium phase transitions in mean field Hamiltonian dynamics in Chaos, Complexity and Transport: Theory and Applications, edited by C. Chandre, X. Leoncini, G. Zaslavsky (World Scientific 2008)
- [81] F. Staniscia, P.H. Chavanis, G. de Ninno, D. Fanelli, Phys. Rev. E **80**, 021138 (2009)
- [82] F. Staniscia, A. Turchi, D. Fanelli, P.H. Chavanis, G. De Ninno, Phys. Rev. Lett. **105**, 010601 (2010)
- [83] F. Baldovin, P.H. Chavanis, E. Orlandini, Phys. Rev. E **79**, 011102 (2009)
- [84] J. Barré, D. Mukamel, S. Ruffo, Phys. Rev. Lett. **87**, 030601 (2001)
- [85] T. Tatekawa, F. Bouchet, T. Dauxois, S. Ruffo, Phys. Rev. E **71**, 6111 (2005)
- [86] P.H. Chavanis, L. Delfini, Phys. Rev. E **81**, 1103 (2010)
- [87] C. Mouhot, C. Villani, [arXiv:0904.2760]
- [88] P.H. Chavanis, in preparation
- [89] Teles *et al.* [44] propose a variant of the Lynden-Bell distribution that gives very good agreement with numerical simulations.
- [90] We shall explain in Sec. II why these control parameters are the proper ones to consider in the Lynden-Bell theory.
- [91] Discrepancies occur for larger values of the magnetization, in particular for  $M_0 = 1$  [32, 70, 76]. This was interpreted as a result of incomplete relaxation in [74]. Chavanis & Campa [77] showed that polytropic (Tsallis) distributions can provide a good description of QSSs in some cases of incomplete relaxation. In their work, Tsallis distributions are justified not by the fact that the system is nonextensive but by the fact that the evolution is non-ergodic (i.e. the system does not mix well).
- [92] In [82], it is concluded that it is possible to measure negative kinetic specific heats in the canonical ensemble when the distribution function is non-Boltzmannian. In the context of Lynden-Bell's statistical theory of violent relaxation relying on the Vlasov equation, the distribution function is non-Boltzmannian (leading to possibly negative kinetic specific heats) but the only physically relevant statistical ensemble is the microcanonical one since the system is isolated (the energy is conserved). If we put the system in contact with a thermal bath as in [83], we break the structure of the Vlasov equation (in the regime where the bath has some influence on the system's dynamics) and the Lynden-Bell theory does not apply anymore. In that case, the distribution becomes Boltzmannian with the temperature of the bath (and the kinetic specific heat is necessarily positive). In other words, we cannot impose the temperature of the Lynden-Bell distribution; the relevant control parameter is the energy. However, it is suggested in [82] that there may exist other situations in which the system is in contact with a thermal bath imposing its temperature while the distribution function is non-Maxwellian. The characterization of this situation is still a matter of investigation.
- [93] Traditionally, the free energy is defined by  $F[f] = E[f] - TS[f]$ . However, the Massieu function  $J[f] = -\beta F[f]$  turns out to be more convenient in the analysis of phase transitions (see, e.g. [7]) since it corresponds to the direct Legendre transform of the entropy with respect to the energy. Since  $F[f]$  and  $J[f]$  are equivalent (recall that  $\beta$  is fixed in the canonical ensemble), we shall often refer to  $J$  as the "free energy" by a slight abuse of language.
- [94] In particular, the thermodynamical specific heat  $C = dE/dT$  is necessarily positive in CE while it can be positive or negative in MCE.
- [95] It can be noted that, in case of *incomplete* relaxation, the initial conditions  $(E, M_0^{(1)})$  and  $(E, M_0^{(2)})$  can lead to different results, although the Lynden-Bell theory leads to the same prediction. This could be interesting to check.
- [96] A similar situation has been observed in [77] for polytropic distributions.
- [97] We should be careful, however, that Staniscia *et al.* [81] do not determine the detailed distribution functions  $f(\theta, v)$  of the inhomogeneous states. It is possible that the Lynden-Bell theory predicts the correct phase transitions in terms of the magnetization although the distribution functions are not exactly given by Eq. (6). This would be interesting to check in future works.